Journal of the European Ceramic Society **16** (1996) 379–384

0955-2219(95)00087-9
0955-2219/96/$15.00

Modern Applications of a New 300 kV Field Emission Transmission Electron Microscope to the Study of Advanced Materials

Y. Bando, K. Kurashima & S. Nakano

National Institute for Research in Inorganic Materials, 1-Namiki, Tsukuba, Ibaraki 305, Japan

(Received 18 April 1995; revised version 19 May 1995; accepted 22 May 1995)

Abstract

Some instrumental features of a new 300 kV analytical transmission electron microscope with a field emission gun and its applications to structure and composition analysis of advanced materials at nanometer scales are given. In the new microscope, a fine electron probe of about 0·5 nm in size with a probe current of about 0·1 nA can be routinely applied for elemental analysis in combination with high resolution lattice imaging. A crystal structure of 33R-AlN polytype is determined from the single atomic layer level analysis using energy dispersive X-ray spectrometry (EDS). It is also shown that a new cubic B–C–N compound is identified to be a diamond-like structure from the observation of lattice image and electron energy loss spectrometry (EELS).

1 Introduction

In recent years, analytical transmission electron microscopes have become a most useful tool in materials science. Energy dispersive X-ray spectrometry (EDS) and electron energy loss spectrometry (EELS) which are attached to the microscope column, can be successfully applied to perform quantitative and qualitative analysis from small volumes in thin specimens.[1–2] The relations between structures and compositions in local areas are then well determined. However, the conventional transmission electron microscope having a thermal emitter of LaB_6 is not always powerful to carry out high spatial resolution chemical analysis at nanometer level regions, because the brightness of the electron source emitter is very limited and then corresponding electron probe current for the nanometer scale probes is too small to perform the elemental analysis.

Since the brightness of the field emission gun is approximately 100 times larger than that of the thermal LaB_6 emission gun, the analytical transmission electron microscope with the field emission gun is very powerful to carry out high spatial resolution analysis at nanometer scales. In the field emission microscope, the very fine electron beam of about 1 nm size with a high current density of about 1 nA can be obtained.[3–5]

In 1993, at the National Institute for Research in Inorganic Materials (NIRIM), a new 300 kV medium voltage analytical transmission electron microscope with a field emission gun was constructed and the high spatial resolution analysis of advanced materials such as silicon nitride and $InFeO_3(ZnO)_{13}$ has been carried out.[6–8] In this paper, the important features of the new microscope are briefly summarized. Also, some applications in the structure and composition analysis of advanced materials, such as aluminum nitride and boron nitride containing carbon, are given. It is shown that the high spatial resolution elemental analysis with EDS and EELS techniques using the fine electron probe of about 0·5 nm diameter are successfully carried out in combination with high resolution lattice imaging. The results of the crystal structure analysis of the 33R-AlN polytype and the new cubic B–C–N compound are described.

2 A New 300 kV Field Emission Analytical Transmission Electron Microscope at NIRIM

2.1 Principal specifications

The main purpose for constructing the new 300 kV analytical transmission electron microscope with a field emission gun, is to carry out ultra high spatial resolution analysis at subnanometer to nanometer scales in combination with high resolution lattice imaging. Some characteristic instrumental features of the new microscope have been already described.[9] The principal specifications of

the new 300 kV field emission microscope are shown as follows:

(1) A stable field emission gun working at 300 kV is required.
(2) In order to reduce .vibration of electron microscope, both high voltage generator and field emission power supply is placed in one tank.
(3) A probe size can be maintained constant at different probe currents.
(4) A minimum probe size must be smaller than 0·5 nm size having a probe current of about 0·1 nA.
(5) A point-to-point resolution must be better than 0·2 nm, in which a double tilt specimen holder can be tilted up to ± 30°.
(6) In order to increase the detection sensitivity for EDS analysis, the X-ray solid angle is larger than 0·20 str.
(7) The peak to the background ratio of the EDS spectra using the Fiori method must be higher than 3700 at 300 kV.
(8) In order to reduce the X-ray cut-off effect due to the specimen holder, a new specimen holder with a Be mount base is designed.
(9) An energy resolution of a zero loss peak must be better than 0·6–0·8 eV at 300 kV.
(10) The image resolution of the scanning transmission electron microscope (STEM) is about 0·34 nm.
(11) Using a liquid helium specimen holder and a high temperature specimen holder, the image resolution at low temperature (15 K) and at high temperature (1300 K) is about 0·23 nm.

The principal specifications described above have been successfully confirmed by experimental observations.[6,9]

2.2 Probe sizes and probe currents produced by thermally assisted type and Schottky type field emission guns

It is well known that there are three types of field emission guns such as the cold-type, the Schottky-type and the thermally assisted-type, which are now used in transmission electron microscopes. The emitter cathodes for the cold-type, the thermally assisted type and the Schottky type were single crystals of a tungsten <310> oriented chip, a tungsten <100)> chip and a tungsten <100) chip coated with zirconium oxide, respectively. In the Schottky type and the thermally assisted type of the field emission guns, the cathode chips were heated at high temperatures of about 1400–1800 K. It is characteristic of these guns that stable emission currents with high total emission currents can

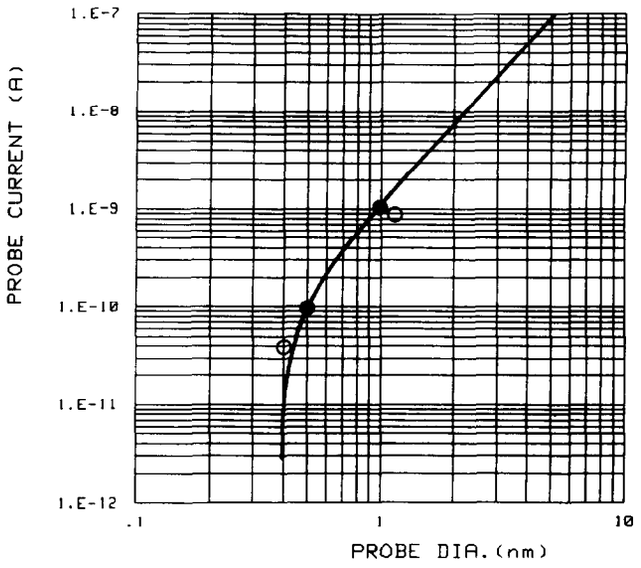

Fig. 1. A calculated probe diameter as a function of probe current at 300 kV. Brightness of electron source for the thermally assisted type and Schottky type field emission gun was considered as 7×10^8 A/cm^{2}st. The minimum probe size was assigned to be 0·4 nm. The observed probe currents for the 0·5 and 1·0 nm probe sizes for the thermally assisted type they were measured as about 0·1 and 1·0 nA, respectively, and for the Schottky type were 0·07 and 0·9 nA for 0·4 and 1·1 nm probe sizes, respectively, in which observed values are marked by dark circles (thermally assisted type) and open circles (Schottky type), respectively.

be produced for a long use over a long period of time. In the new microscope, we used the thermally assisted type field emission gun in a first installment and then the gun was changed to the Schottky type.

The electron probe diameter, D at the specimen point were calculated by the following equations.

$$D = (D^2_g + D^2_{Cs} + D^2_{Cc} + D^2_d)^{1/2}$$

Here D_g, D_{Cs}, D_{Cc} and D_d indicate the Gaussian image of the emitter source, the minimum disk broadening caused by a spherical aberration (Cs), a chromatic aberration (Cc) and a diffraction aberration (d), respectively. A result of the calculation of the probe diameter as a function of the probe current is shown in Fig. 1. In the calculation, the brightness of the field emission gun is considered as 7×10^8 A/cm^2· str at 300 kV for both the thermally assisted type and the Schottky type. The minimum probe size was assigned to be about 0·4 nm at 300 kV.

Figure 2 shows a profile of a minimum probe size for the Schottky type field emission gun. The total emission current was 130–150 uA with an extraction electrode potential of 3·1 kV, an electrostatic lens potential of 6·6 kV, a filament heating current of 2·3 A. A half-width of the minimum probe size recorded was about 0·4 nm. The minimum probe size for the thermally assisted type was also observed to be 0·4 nm. These observa-

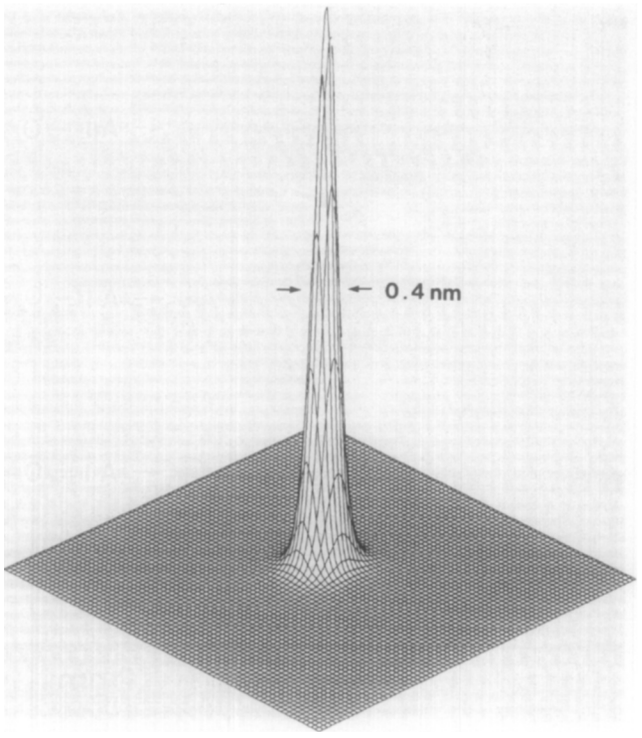

Fig. 2. A profile of minimum probe size for the Schottky type field emission gun, recorded by an imaging plate. The minimum probe size was observed to be about 0·4 nm.

tions agreed well with the calculation of Fig. 1. The probe currents were also measured by using a Faraday cup. The probe currents for the Schottky type were about 0·07 nA and 0·9 nA for the probe sizes of 0·4 nm and 1·1 nm, respectively and for the thermally assisted type they were about 0·1 nA and 1·0 nA for the probe sizes of 0·5 nm and 1·0 nm, respectively. These observed values are indicated in Fig. 1. The probe currents between the two different guns were almost the same in such small probes.

3 Applications in the Study of Advanced Materials

3.1 Monolayer level analysis of AlN polytype

Aluminum nitride (AlN) is a very useful material for the use of substrate in LSI devices instead of alumina, since it shows a high thermal conductivity. This compound reacts easily with oxygen at high temperatures to form aluminum oxynitride or aluminum silicon oxynitride, which are known as compositional polytypes or polytypoids.[10,11] It is characteristic of present polytypes that the composition varies with a periodicity of the *c*-axis. In the $AlN–Al_2O_3$ system, polytypes such as 12H, 15R, 33R, 39R and 32H have been already observed[12–14] and its composition was considered as a general chemical formula of $mAlN–Al_2O_3$, where m is an integer. From the X-ray powder diffraction study, the structure is considered to be AlN_4 (Al–N)

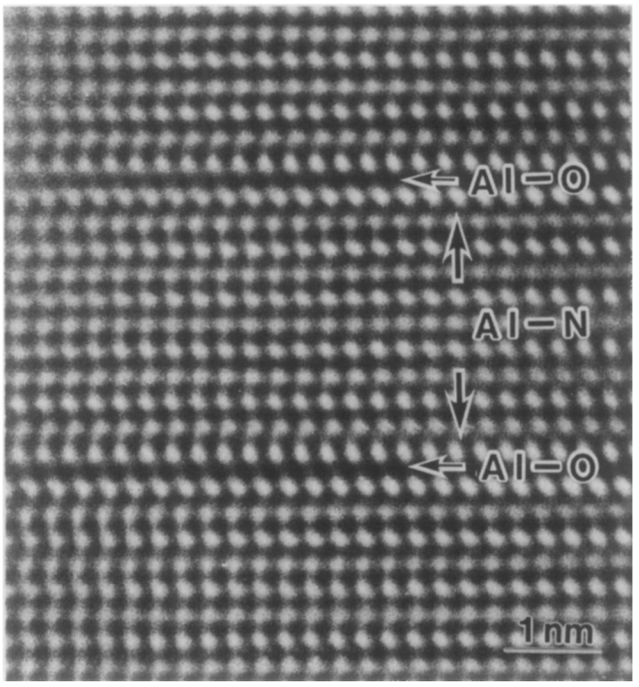

(a)

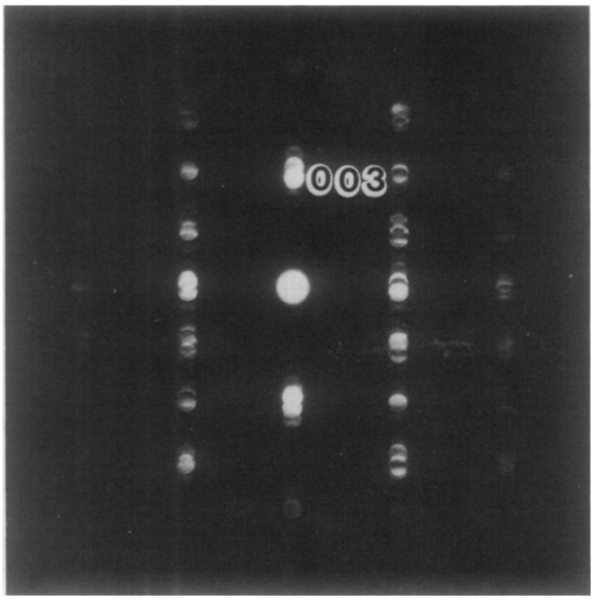

(b)

Fig. 3. A crystal structure image of 33R-9AlN–Al_2O_3 (a) and corresponding nano-area electron diffraction pattern (b). The image was observed at Scherzer defocus. The incident electron beam was normal to the (110) plane. Each of the Al atoms was well resolved as dark dots in the image, but the N and O atoms were not imaged.

tetrahedral layers interleaved with AlO_6 (Al–O) octahedral layers. It is speculated that a part of the nitrogen atoms is replaced by oxygen atoms to form Al–O layers. Since identification between oxygen and nitrogen atoms is difficult in X-ray diffraction, their distribution is not well understood.

Figures 3(a) and (b) shows a crystal structure image of 33R polytype and its corresponding nano-area electron diffraction pattern, respectively. The structure image was observed at

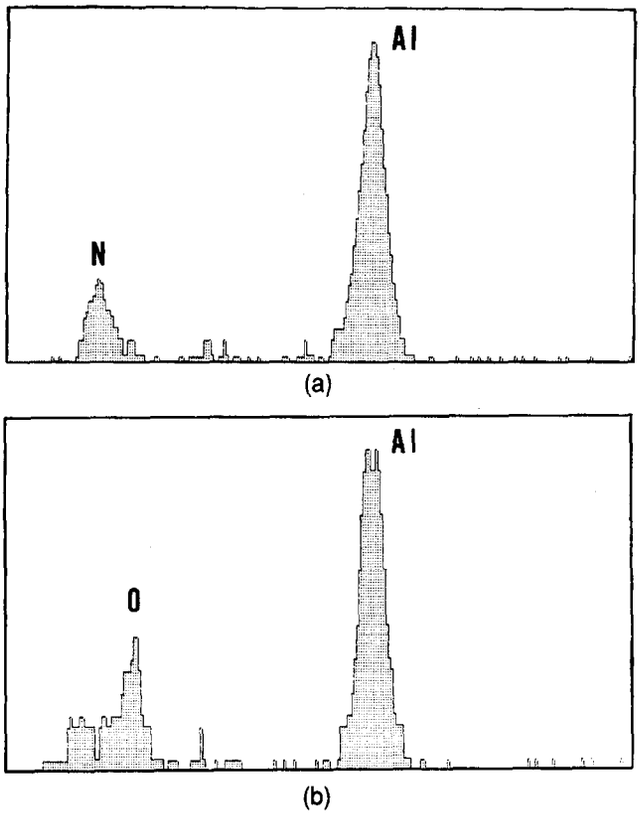

Fig. 4. EDS spectra, obtained from one of the atomic layers marked as Al–N (a) and Al–O (b) in Fig. 3. The probe size was 0·5 nm and the exposure time was 20–30 s.

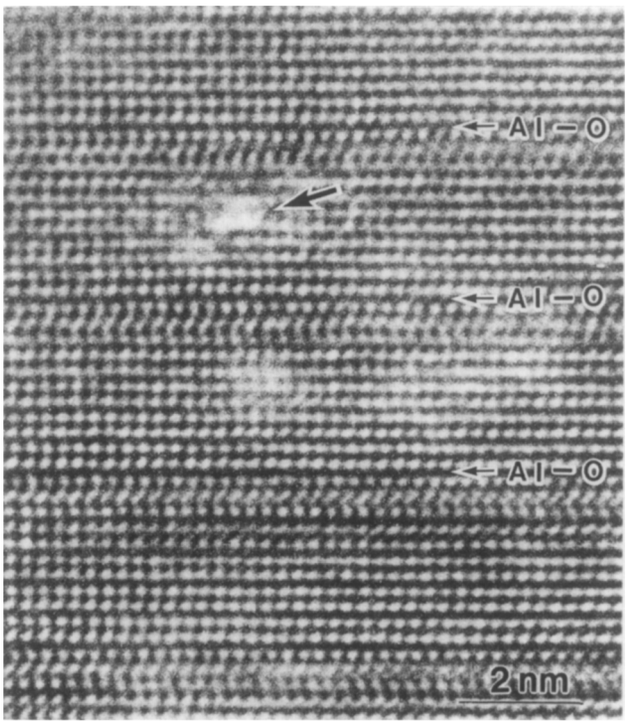

Fig. 5. Radiation damage of the 33R-9AlN–Al_2O_3. A small hole of about 1 nm diameter, which is marked by an arrow was selectively formed with the layers of Al–N during the observation of the EDS point analysis.

Scherzer defocus of about 56 nm. The incident electron beam was normal to the (110) plane. The results of electron diffraction indicates that the crystal is 33R type with lattice parameters a = 0·308 nm and c = 8·69 nm. In the image, each of the aluminum atoms site appeared as dark dots, while those of the N and O atoms were not imaged. The separation between the dark dots normal to the *c*-axis is 0·26 nm.

A chemical analysis using the EDS method was carried out in combination with high resolution lattice image, where the fine electron probe of about 0·5 nm size was focused on each single atomic layer as indicated in the figure. Figures 4(a) and (b) show EDS spectra, obtained from the layers marked as Al–N and Al–O, respectively. The acquisition time was about 20–30 s. Every 10 s, the focused probe position was confirmed to be constant during the observation. In the spectrum in Fig. 4(a), nitrogen and aluminum X-ray peaks were clearly observed and almost no oxygen peaks were detected. While in the spectrum in Fig. 4(b), the oxygen peak was identified as well as the aluminum peak with a the weak nitrogen peak. This elemental analysis confirms that oxygen atoms are not randomly distributed among the nitrogen layers, but they are ordered to form Al–O layers.

The crystal structure of 33R type is then derived. The 33R aluminum oxynitride polytype consists of 9 layers of AlN_4 tetrahedral layers interleaved with 2 layers of AlO_6 octahedral layers along the *c*-axis. From the rhombohedral symmetry, the structure unit is repeated three times to give a total of 33 layers. The chemical composition is then assigned to be 9AlN–Al_2O_3, which is consistent with the general chemical formula of m = 9.

During the observation, the specimen often suffered radiation damage due to a focused strong beam irradiation. Figure 5 shows a high resolution lattice image of 33R type after the radiation damage. After about 30 s exposure of the fine electron beam to the specimen, small holes measuring a few nanometers were formed. These small holes were only introduced into the areas of Al–N layers and no holes were formed at the layers of Al–O. This means that selective mass loss has occurred due to electron beam irradiation effect. The Al–N layers are more easily attacked than those of Al–O by the electron beam bombardment.

3.2 Identification of a cubic B–C–N compound

Recently, one of the present authors prepared a cubic phase of B–C–N compound under the conditions of high pressure (7 × 7 GPa) and high temperature (2150–2400°C).[15] A graphite BC_2N compound was transformed into the cubic B–C–N phase with minor phases of cubic BN and diamond under such conditions without using an additive. However, no direct evidence of the cubic B–C–N phase has been obtained.

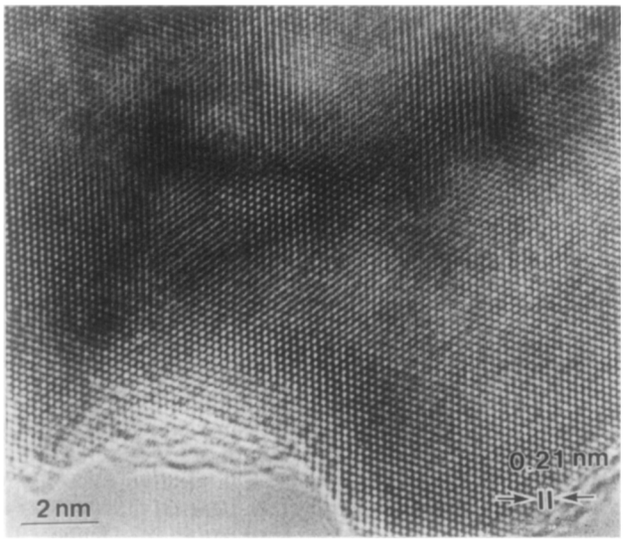

(a)

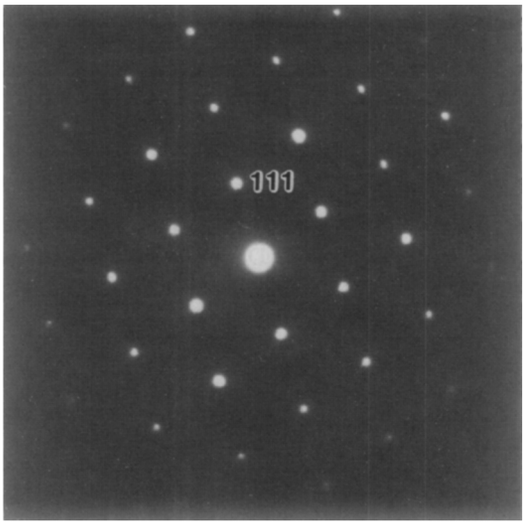

(b)

Fig. 6. A high resolution lattice image of a new B–C–N crystal (a) and its corresponding electron diffraction pattern (b). The crystal was assigned to be cubic with lattice parameter a = 0·36 nm. The lattice separation of about 0·21 nm corresponds to cubic (111) plane.

The specimens contained small crystal fragments of a few tens nanometer scales. Figures 6(a) and (b) show a high resolution image of the specimen fragment and its corresponding electron diffraction pattern, respectively. The electron diffraction pattern was assigned to be cubic (110) plane. It is then concluded that the crystal is cubic with lattice parameter a = 0·36 nm. In the high resolution image of Fig. 6(a), a cubic packing of white dots having a separation of about 0·21 nm was well observed. This lattice separation corresponded to the cubic (111) plane. The result of the lattice image also suggests that the crystal is a diamond-like structure.

In order to confirm the chemical composition of the specimens, an EELS spectrum was obtained from the specimen fragment as shown in Fig. 6. The result is shown in Fig. 7. In the spectra, loss

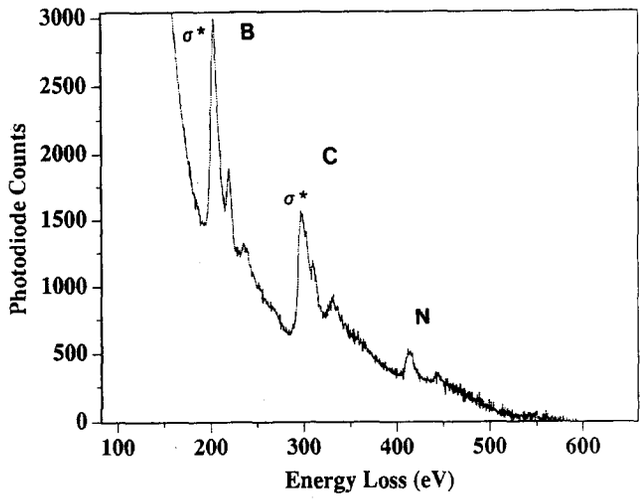

Fig. 7. An EELS spectrum, obtained from the edge part of the specimen as shown in Fig. 6. The δ^* edges were clearly observed with the absence of π^* edges. The crystal was then assigned to be B–C–N compound with a diamond-like structure.

peaks located at about 188, 283 and 402 eV corresponded to k edges of boron (B), carbon (C) and nitrogen (N), respectively. The characteristic δ^* peaks were present and π^* peaks were not observed at the near edges of B and N. This indicates that the crystal is not a graphite-like but a diamond-like structure.

During the observation, the present cubic B–C–N phase transformed into a hexagonal phase due to heating effect by strong beam irradiation. Figure 8(a) shows a high resolution lattice image of the B–C–N crystal showing the cubic to hexagonal transformation. The specimen was the same as that of Fig. 6. After the strong beam irradiation, the graphite-like structure having the separation of 0·34 nm of (002) lattice plane was newly formed. It grew from the edge part of the fragment. An EELS spectrum, observed from the graphite-like structure is shown in Fig. 8(b). Its fine structure is very different from that of Fig. 7 and the characteristic π^* peak corresponding to the graphite-like structure was clearly observed, suggesting that the specimen is the hexagonal B–C–N compound. It is very characteristic in the image that the graphite-like layers were very irregular and curled, where the edge dislocation is indicated by an arrow in the figure. These features correspond to a turbostatic layered structure.

It should be noted that the hexagonal B–C–N have an epitaxial relation with the cubic B–C–N phase. From the observation of the lattice image as shown in Fig. 8(a), the lattice relations between them are as follows.

$^{(101)}$hexagonal$^{//(111)}$cubic
$^{[010]}$hexagonal$^{//[1\bar{1}0]}$cubic

A detailed analysis of the cubic B–C–N crystal will be published elsewhere.

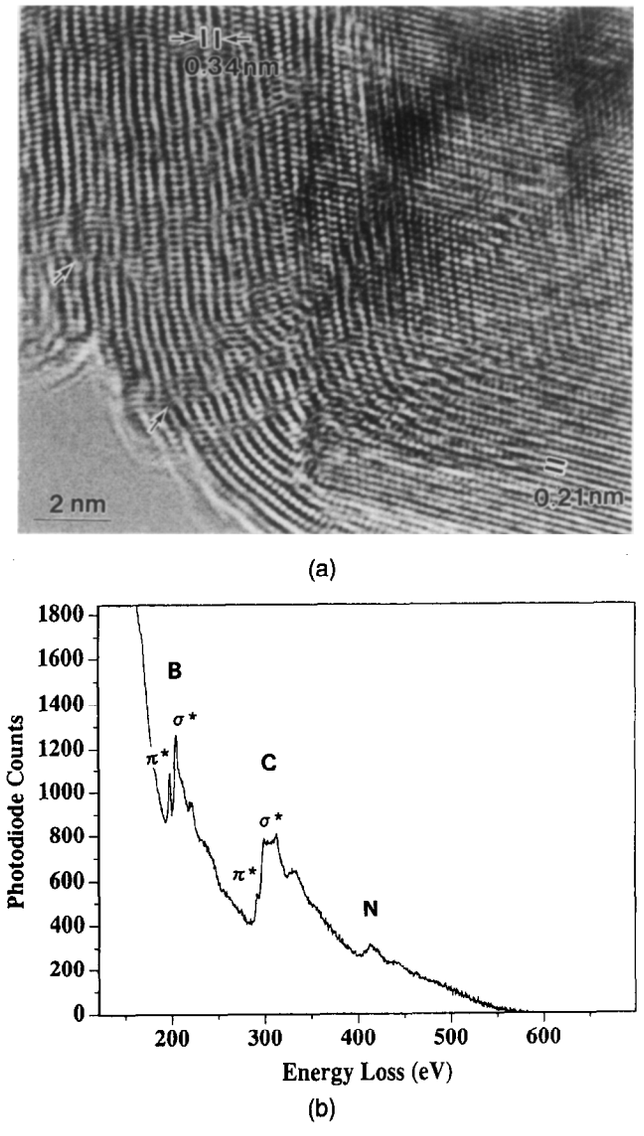

Fig. 8. A high resolution lattice image of the B–C–N crystal (a), where the cubic structure changed into the hexagonal structure after the radiation damage, and its corresponding EELS spectrum (b). The specimen was the same as that of Fig. 6. After the beam heating by the strong beam irradiation, the graphite-like structure having 0·34 nm lattice separations was newly formed. The edge dislocation is indicated by an arrow. The characteristic π^* peak was well observed in (b).

4. Conclusion

The new 300 kV analytical transmission electron microscope with a field emission gun, which has been recently developed in NIRIM, is successfully applied to carry out high spatial resolution analysis of advanced materials at subnanometer to nanometer level using EDS and EELS techniques. The crystal structure of 33R polytype was determined in the combination of the lattice image and the point analysis of the EDS. The new phase of cubic B–C–N was also identified from the EELS observation.

Acknowledgements

The authors thank Drs M. Akaishi, T. Sasaki and S. Yamaoka for supplying the specimens and also valuable discussions. They also thank Mr Y. Kitami, NIRIM, and Mr M. Tomita and K. Kawasaki, JEOL, for the support of the experiment.

References

1. Bando, Y., Analytical transmission electron microscopy of materials in Japan. *J. Electron Microsc.*, **S58** (1989) 81–9.
2. Bando, Y., Analytical transmission electron microscopy in materials science. *Mater. Trans. JIM*, **31** (1990) 538–44.
3. Isakozawa, S., Sato, Y., Kashikura, Y., Kubo, T., Hashimoto, T., Takahashi, T., Ichihashi, M. & Murakoshi, H., Development of 200 kV field emission TEM. In *Proc. 47th Annual Meeting Electron Microscopy Society of America*, Ed. The Organizing Committee, San Francisco Press, San Francisco, 1989, 112–13.
4. Tomita, T., Katoh, S., Kitajima, H., Kokubo, Y. & Ishida Y., Development of field emission gun for high voltage electron microscope. In *Proc. XIIth Int. Congr. for Electron Microscopy*, Ed. The Organizing Committee, San Francisco Press, San Francisco, 1990, 94–5.
5. Coene, W., De Jong, A. F., Lichite, H., Op de Beek, M., Tietz, H. & Van Dyck, D., FEG-TEM: The route to HRTEM. In *Proc. 50th Annual Meet. Electron Microscopy of America*, Ed. The Organizing Committee, San Francisco Press, San Francisco, 1992, 100–1.
6. Bando, Y., Kitami, Y., Tomita, T., Honda, T. & Ishida Y., A newly developed 300 kV field-emission analytical transmission electron microscope. *Jpn. J. Appl. Phys*, **32** (1993) L1704–6.
7. Bando, Y., Subnanometer level analysis by 300 kV FE-ATEM. In *Proc. 13th Int. Congr. for Electron Microscopy*, Ed. The Organizing Committee, Les editions de physique, Paris, 1994, 591–4.
8. Bando, Y., Suematsu, H. & Mitomo, M., Grain boundary phase analysis of silicon nitride by a newly developed 300 kV field emission electron microscope. In *Mat. Res. Soc. Symp. Proc. Vol. 346*, 1994 Materials Research Society, 1994, 733–8.
9. Bando, Y., Kitami, Y., Kurashima, K., Tomita, T., Honda, T. & Ishida, Y., Development and application of 300 kV field emission analytical transmission electron microscope, *Microbeam Analysis*, **3** (1994) 276–86.
10. Jack, K. H., Nitrogen ceramics. *Trans. J. Brit. Ceram. Soc.*, **72** (1973) 376–84.
11. Bando, Y., Mitomo, M., Kitami, Y. & Izumi, F., Structure and composition analysis of silicon aluminum oxynitride polytypes by combined use of structure imaging and microanalysis. *J. Microscopy*, **142** (1986) 235–46.
12. Sakai, T., Hot-pressing of the AlN–Al_2O_3 system, Yogyo-Kyokai-Shi, 86 (1978) 125–30.
13. Bartram S. F. & Slack. G. A., $Al_{10}N_8O_3$ and $Al_9N_7O_3$, two new repeated-layer structures in the AlN–Al_2O_3 system. *Acta Cryst.*, **B35** (1979) 2281–3.
14. Van Tendeloo, G., Faber K. T. & Thomas, G., Characterization of AlN ceramics containing long-period polytypes. *J. Mater. Sci.*, **18** (1983) 525–32.
15. Nakano, S., Akaishi, M., Sasaki, T. & Yamaoka, S., Segregative crystallization of several diamond-like phases from the graphitic BC_2N without an additive at 7·7 GPa, *Chem, Mater.*, **6** (1994) 2246–51.